$Ti_3C_2T_x$ MXene-Au nanoparticles doped polyimide thin film as a transducing bioreceptor for real-time acoustic detection of carcinoembryonic antigen

P J Jandas[1,2,3], K Prabakaran[2,3], Jingting Luo[2]*, Chen Fu[2], Yong Qing Fu[4], Derry Holaday M G[5]

[1]Department of Polymer Science and Technology, Cochin University of Science and Technology, Kochi-682022, Kerala, India.

[2]Shenzhen Key Laboratory of Advanced Thin Films and Applications

College of Physics and Optoelectronic Engineering, Shenzhen University, 518060, Shenzhen, PR China

[3]Key Laboratory of Optoelectronic Devices and Systems of Ministry of Education and Guangdong Province, College of Optoelectronic Engineering, Shenzhen University, 518060, Shenzhen, PR China

[4]Faculty of Engineering and Environment, Northumbria University, Newcastle upon Tyne, NE1 8ST, UK

[5]Department of Chemistry, University of Calicut, Thenhipalam, Kerala - 673635, India.

Dr. P J Jandas
Department of Polymer Science and Technology
Cochin University of Science and Technology
Thrikkakara, Kalamassery, Kochi, Kerala – 682022
India
Ph. +91 9746173210
Email: drjandasjanan@gmail.com

Abstract

$Ti_3C_2T_x$ MXene was synthesized and the 2D layers were hybridized with Au nanoparticle (AuNP) through *the in-situ* method. The study was successfully prepared MXene 2D layer and the same was TEM captured as well. Polyimide/MXene-AuNP (PI/Mxene-AuNP) transducing conducting nanocomposite thin film was synthesized and evaluated the new material's capability to use as a transducing thin film for biosensing application. The bioreceptor was prepared on the delay line area of the SAW device by covalently immobilizing mouse monoclonal antibody of carcinoembryonic antigen (CEA) through the thioglycolic acid arm linker mechanism. Immunoassay analysis has suggested that the biosensor responds linearly with the increase in the concentration of the CEA sample. The limit of detection was observed at 0.001 ng/ml. The insertion loss of the bioreceptor was recorded at 10 dB, which also mattered in the high sensitivity of the biosensor. The biosensor has shown excellent selectivity within the environment of other common tumour markers and was stable for 75 days under periodical testing conditions. Clinical serum samples were analyzed successfully and the results were compared with values obtained through the ELISA method.

Keywords: MXene; $Ti_3C_2T_x$; AuNP; Biosensor; CEA; SAW.

1. Introduction

2D nanomaterials are one of the hot topics today for various high-end applications [1]. The materials find applications in various biomedical devices and ecological monitoring. The materials find application in biosensors for a variety of perspectives including therapeutic, diagnosis, toxicity analysis, and DNA, protein, and living cell detection. The unique chemical, physical and optical properties of these 2D materials have a critical influence on the performance characteristics of the biosensors. Biosensors for cancer diagnosis are one popular area of research utilizing the advent in 2D material developments [2]. These biosensors are utilizing the excellent transducing capability of 2D materials which can transfer the chemical changes happening on the electrode surface during any biosensing or immunosensing process into detectable signals to provide excellent sensitivity to the device [3]. Graphene oxide (GO), MXenes, 2D MoS_2, black phosphorus, etc alone or in combination with other nanomaterials are in high demand for biosensing applications today [4].

Today cancer is one of the prime reasons for premature death [5]. Any human body affected by cancer always associated with a biomarker in the form of DNA, RNA, proteins, lipids, and metabolites. These biomolecules can be detected and estimated as an indicator for specific cancer, patient's clinical stages, and the output data helps to develop adaptive therapeutic strategies [5]. However, the complex biomolecular structure of nucleic acids, tumor heterogeneity born specific protein signatures, and very low concentrations in the analyte sample restrict the sensitive detection of cancer biomarkers [6]. Experimental studies of biosensing strategy based on electrochemical, optical, and mass detection of these biomarkers are reported in many reports [7]. Preparation of biosensors for the selective and sensitive estimation of tumor marking protein antigens through antibody immobilized bioreceptor is

popular today [7]. However, the method demands materials that are capable of easy and effective transduction of electromagnetic signals during the analysis. 2D nanosheets of MXenes are popular today as highly promising electrode materials for biosensing applications owing to their specifically laminated structures and astonishing properties [8]. MXenes show excellent electrical conductivity and electromagnetic signal transduction capability [9]. MXenes are early transition metal carbides or nitrides prepared by etching "A" element from the MAX phase compounds (M-Early transition metal, A-group III or IV element, X-Carbon). MXenes have the exclusive synergy of properties, including high electrical conductivity, excellent mechanical properties, high negative zeta-potential, and easily functionalizable surfaces. These unique combinations of properties make the material attractive and opens the application in colloidal forms after coupling with organic moieties [10]. $Ti_3C_2T_x$ (T = F, OH) is popular among the various MXenes due to its less complex method of preparation, high conversion rate, and excellent output properties including for biosensing and supercapacitance applications [11].

Polymers and polymer matrices coupled with nanomaterials are attracting researchers as effective bioreceptors, irrespective of the detecting technology of biosensing in recent years. A new category of macromolecules known as intrinsically conducting polymer or electroactive conjugated polymers (extended π-conjugation along the polymer backbone) has recently been attracted by the researchers due to their unique electrochemical properties including excellent electrical conductivity, poor ionization potential, outstanding electronic affinities, and good optical properties. [12-13]. Polyenes and polyaromatics such as polyacetylene, polyaniline (PANI), polypyrrole (Ppy), polythiophene, poly (*p*-phenylene), poly (phenylene vinylene) are well-known names in the conducting polymer family [14].

Conducting polymers with two-dimensional (2D) nanomaterials with planar topology and thickness of nanometer range find attention from the researchers as a potential transducing

bioreceptor material for piezoelectric biosensors [15]. Piezoelectric biosensing methods like quartz crystal microbalance (QCM) and surface acoustic wave (SAW) biosensors find attractive to the researchers working in the area of biosensors over the popular methods like electrochemical and optical methods due to high sensitivity, stability, and consistency in the output results [15]. In the present study, a transducing thin film of polyimide/MXene-AuNP (PI/MXene-AuNP) nanocomposite was synthesized and its utilization as a novel bioreceptor for the selective detection of CEA was studied. The novel material has been synthesized based on the hypothesis that the inherent qualities of PI conducting polymer coupled with MXene 2D layers can give exceptional biosensing performance. Besides, AuNP can provide stability to the bioreceptor through creating strong covalent interaction between polymer nanocomposite thin film and anti-CEA via thioglycolic acid arm linker [25]. MXene $Ti_3C_2T_x$ was synthesized using selective etching of Al from Ti_3AlC_2 MAX-phase through the HF method. AuNP was allowed to grow on the 2D MXene layers in the next step and MXene-AuNp was incorporated within the previously synthesized polyamic acid precursor. A thin film was prepared on the SAW device and polymerized to PI/MXene-AuNP nanocomposite under controlled thermal treatment. By varying the viscosity of the precursor solution and spin coating parameters, the thickness of the thin film was controlled. Further, the mouse monoclonal antibody of CEA (anti-CEA) was immobilized covalently on the thin film using the thioglycolic acid arm linker. The prepared boireceptor was stored in sterile conditions at 4°C and used for immunoassay analysis using a specially prepared microfluidic chamber connected with a SAW analyzer. The LOD, saturation points, and sensitivity were evaluated. Selectivity, stability, and real-time analysis also were conducted.

2. Experimental

2.1. Materials

N, N dimethylethanolamine (DMEA), pyrometallic dianhydride (PMDA), 4, 4'oxydianiline (ODA), N-methyl pyrrolidone (NMP), TiAlC, thioglycolic acid, ethyl-dimethyl-aminopropyl carbodiimide (EDC), N-Hydroxy Succinimide (NHS), sodium citrate, $HAuCl_4$.$3H_2O$, human CEA, triethylaminopropoxysilane (TAPS), mouse monoclonal antibodies to human CEA (as per the reference ELISA kit), L-Tryptophan, AFP, CA125, and phosphate buffer (PBS, 0.01 M, pH 7.2) were obtained from Sigma Aldrich. CEA was assessed for activity using ELISA tests. Bovine serum albumin (BSA) was obtained from Sinopharm Chemical Reagent Co., Ltd. China. Clinical serum samples were collected from the Second People's Hospital, Shenzhen, China.

2.2. Synthesis of MXene-AuNP nanomaterials incorporated PI nanocomposite

PAA precursor was synthesized as per our previous study [26]. $Ti_3C_2T_x$ MXene was synthesized from Ti_3AlC_2 MAX phase by treating it with 50% concentrated hydrofluoric acid for 3 days at room temperature under stirring with a Teflon-coated magnetic bar at 300 rpm. The resulting product was washed using DI water and centrifuged at 10000 rpm till the pH of the supernatant solution reached around 6. The solution was further sonicated for 1 hour in an ice bath. The MXene powder obtained was filtered using a Celgard porous membrane and washed with DI water followed by absolute alcohol. The resultant powder of few-layer MXenes was dried under vacuum for 24 h. 0.05g of MXene was then taken in an RB flask containing 25 ml of DI water. The mixture was heated to 90°C and added 2.5 ml of 10.35 mg/ml of sodium citrate followed by 1 ml of 5 mg/ml aqueous solution of $HAuCl_4$. $3H_2O$ for 15 minutes. The resulting solution containing Au nanoparticle embedded MXene (MXene-AuNP) nano-cluster was cooled, filtered, and washed with DI, followed by absolute alcohol. Finally, the nanoparticles were dried in a vacuum oven at 80°C and stored in sterile conditions.

2.3. AuNP-MXene/PI thin-film based Bioreceptor preparation

Precursor solution of polyimide in DMAc was added to MXene-AuNP (0.1% mixture in DMAc) and sonicated for 1 hour. The nanocomposite precursor was coated on the delay line (1 mm x 5 mm) of the SAW device by placing 15 μL of the mixture followed by spin coating. Spin coating parameters and viscosity of the precursor were varied to obtain an optimum thickness for transducing thin film. The SAW device was fabricated based on or previous experiments [25]. Spin coating parameters were optimized at 12000 rpm for 45 seconds to maintain a thickness of 600 ± 50 nm after thermal treatment. The transducing thin film was conditioned at room temperature for 24 hours after cleaning with 1N HCl and DI water. Thioglycolic acid was allowed to react with the AuNP by dropping 10 μL of the reagent on the nanocomposite thin film and incubated for 3 hours. The thioglycolic acid end has been activated before receiving the antibody by making an activated complex with ethyl-dimethyl-aminopropyl carbodiimide (EDC) - N-Hydroxy Succinimide (NHS) reactants. This complex structure has been further treated with the antibody (75μg/ml) to form the final bioreceptor. The contact time was optimized at 3 hours. The surface was cleaned using 1 M ethanolamine (pH 8.0) DI water, dried, and stored at 4°C. The concentration of the anti-CEA was optimized after several trials using various concentrations ranging from 10 – 500 μg/ml.

2.4. Biosensing immunoassay analysis

The method of immunoassay analysis followed in the study is represented in Scheme 1. Before the immunoassay analysis, we have designed and fabricated a microfluidic sample analyzer device internally to facilitate easy and proper interaction between the receptor and analyte during the immunoassay analysis. The device has 3 channel sample passage system which can be connected with the SAW device, and the output device, the network analyzer [25]. As the initial stage of analysis, each bioreceptor was exposed to bovine serum albumin (BSA) to minimize undefined capture on the anti-CEA bioreceptor. To understand the sensitivity and limit of detection (LOD) of the biosensor we allowed a fixed volume of CEA

samples to flow through the microfluidic chamber. The volume was fixed because each test needs to be saturated by forming a stable plateau of sensing response. The stock solutions of CEA in PBS with concentrations varying from 0.1 ng/ml to 130 ng/ml were analyzed. A network analyzer, Keysight Technologies, E5071C was used to record the output signals of the immunoassay analysis. Also, the microfluidic chamber was connected with an automated system of sample inlet which allows a steady flow rate. This can minimize the noise formation due to the variation in the rate of flow of the sample. The flow rate was optimized at 0.075 ml/minute.

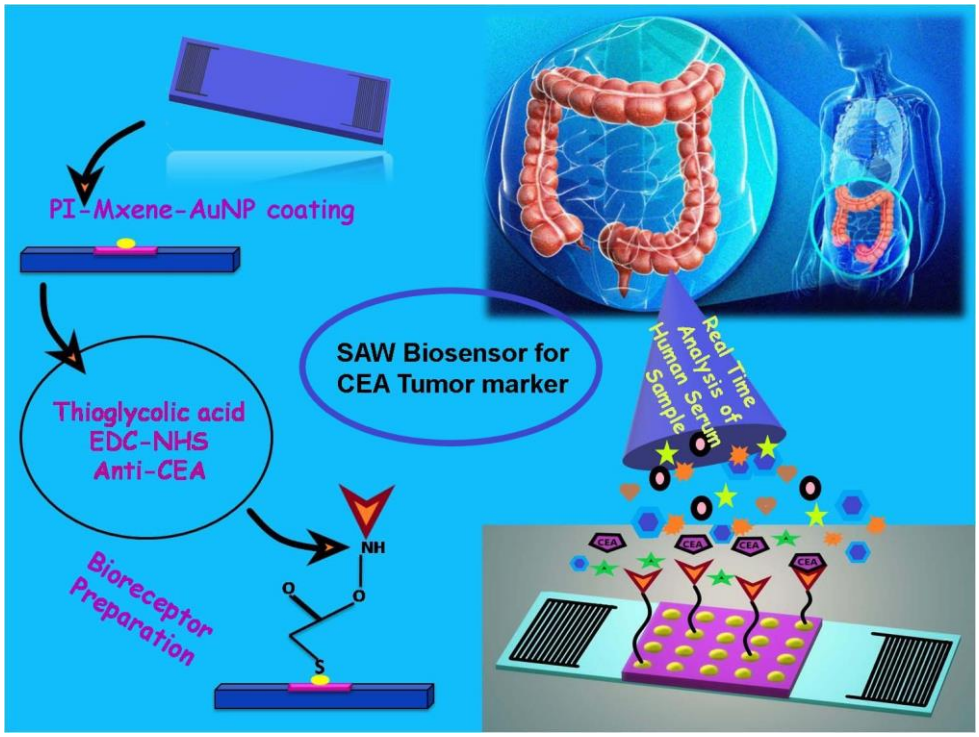

Scheme 1: Basic strategy used for immunoassay analysis

5 iterations of each analysis were conducted and regeneration of the bioreceptor was performed after each analysis cycle after PBS run [26]. Real-time analysis was conducted using clinical serum samples and selectivity evaluated using CEA mixture with other common tumor marking proteins such as alpha-1-fetoprotein (AFP), cancer antigen 125 (CA125), and L-tryptophan. The long-term evaluation capacity was tested by periodical

testing every 5 days till a steep depression in properties observed. The devices were stored at 4 °C and 50 ± 5% relative humidity.

3. Result and Discussion

3.1. Morphology of nanoparticles and polymer nanocomposite

TEM images of MXene 2D nanolayers and MXene-AuNP are given in Figure 1a. Few layer MXenes were successfully prepared through the aforementioned method by the removal of Al^{3+} ions from the MAX phase. However, the study has significant achievement as the method also leads to the formation of MXene 2D layers which is given in figure 1a. TEM analysis has given insight into the formation of AuNP on the MXene 2D surface as well. The AuNP particles of around 10 nm diameter are identifiable on the MXene surface. This has been confirmed using the elemental mapping method. The results suggest maximum removal of Al^{3+} ions in the final material and the formation of a few layers MXene as well. Elemental mapping has also confirmed the formation of AuNP particles on the MXene layers. In a fixed region of 50 nm the elemental density of C, O, Ti, Al, and Au are given in the figure and, understandably, the number density of Al^{3+} is very low as compared to the other elements including Au, Ti, O, and C.

XRD patterns of MAX phase, MXene, and MXene-AuNP are given in Figure 1b. MAX phase has distinctive characteristic peaks at 33°, 39°, and 43°. The peaks around 33° and 43° of the MAX phase were absent in the MXene XRD pattern. The (002) peak in the MXene was shifted towards the lower angle and broadened as compared to the MAX phase. The intensity of the (104) peak at 39 reduced considerably for the MXene XRD pattern [16]. The observations suggest the successful removal of Al^{3+} ions and the formation of few-layer MXene particles [16]. The presence of AuNP was identified through its signature peaks indexed at (111), (200), (220), (311), and (222) reflections [17]. Using the Scherrer equation the average thickness of the MXene layers was calculated as 46 nm. SEM figures (Figure 1c)

further confirm the formation of MXene and MXene-AuNP. The MXene with few layers and an average thickness dimension of 40 nm was imaged. The AuNP formed on the MXene surface was identified as well. The AuNP has an average diameter of 5-10 nm.

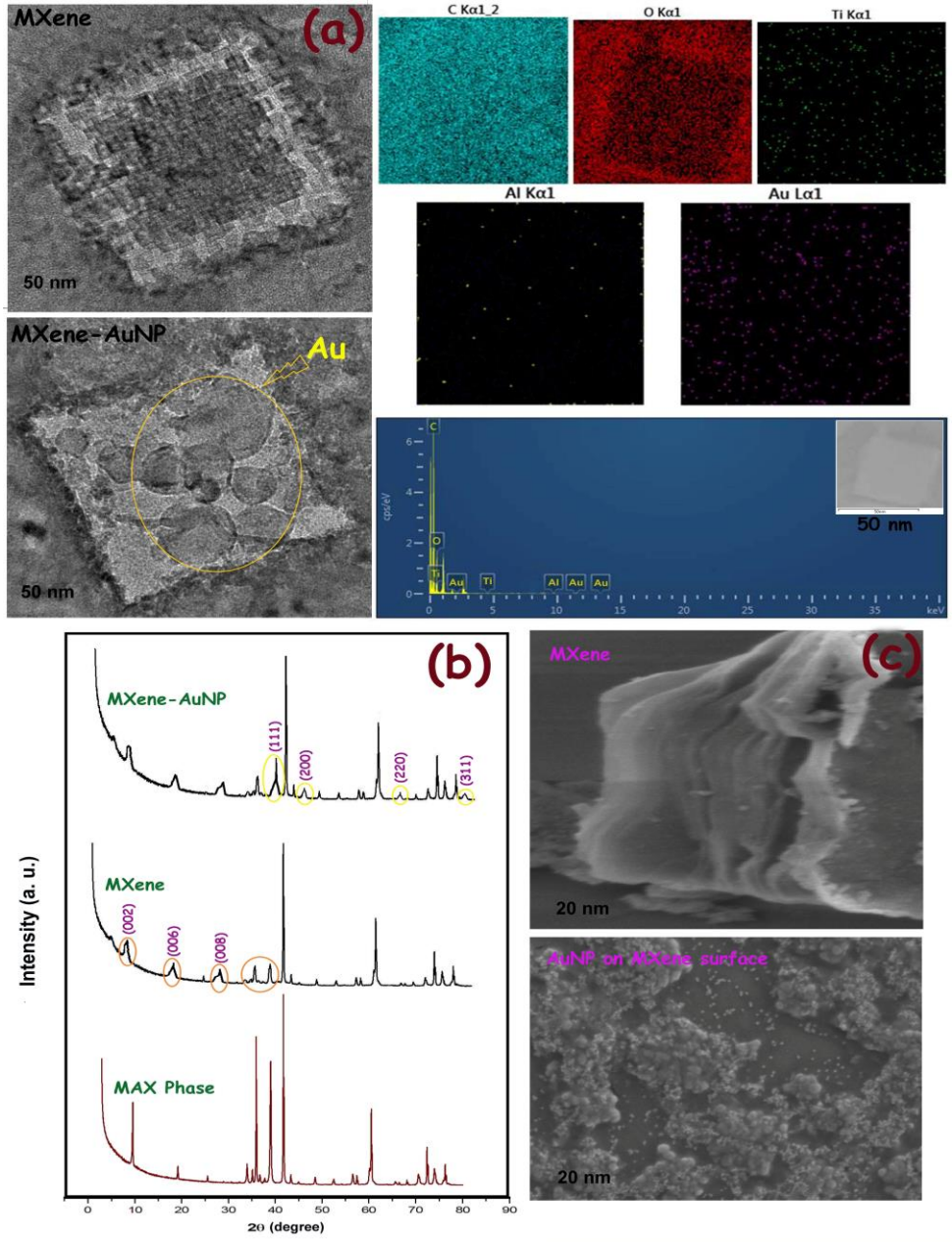

Figure 1: Morphology **(a)** TEM of MXene and MXene-AuNP along with elemental mapping **(b)** XRD MXene and MXene-AuNP and **(c)** SEM of MXene and MXene-AuNP

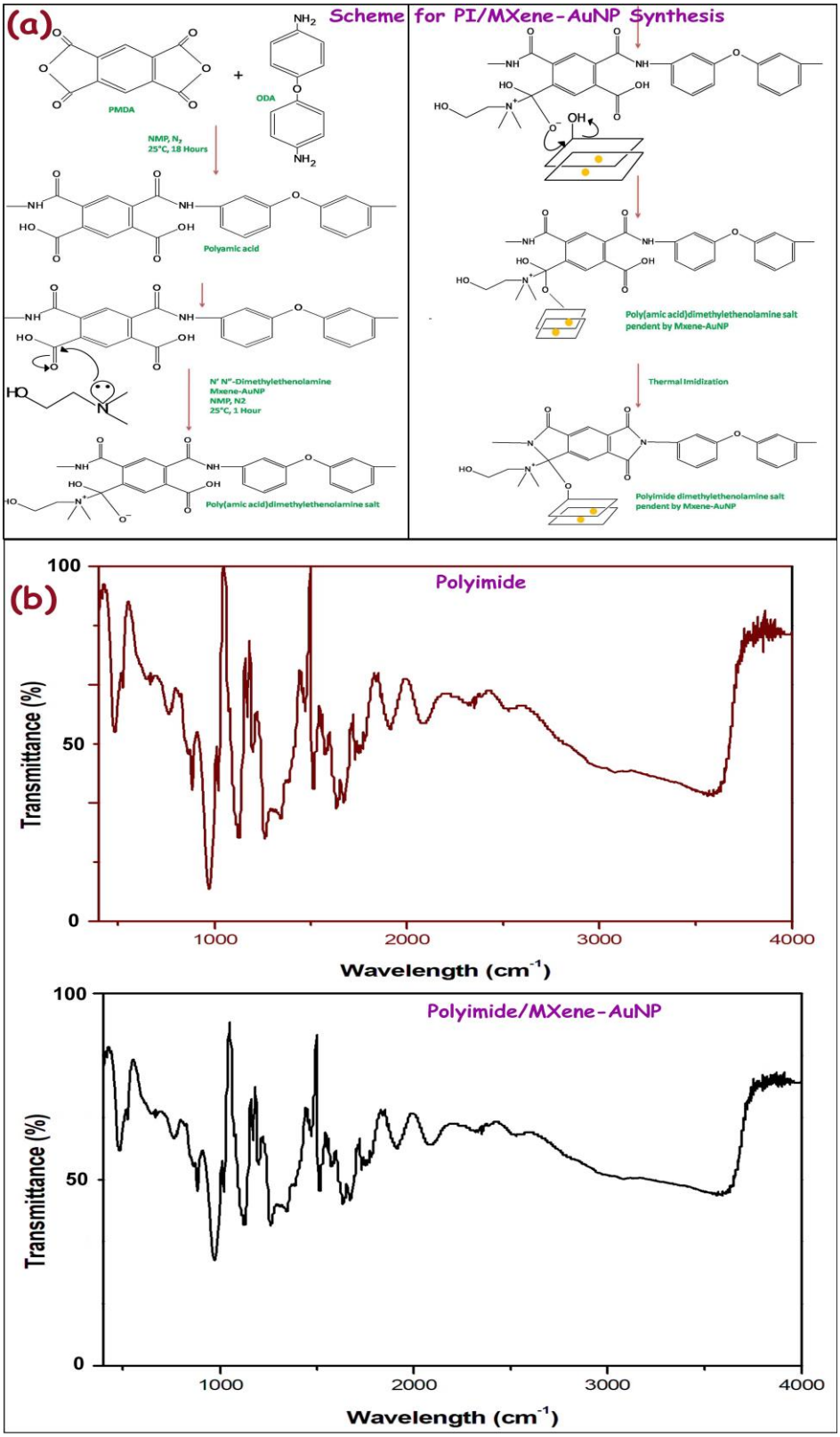

Figure 2: (a) Scheme for PI nanocomposite synthesis **(b)** FT-IR spectra of PI and PI/MXene-AuNP

Further, the PI nanocomposite was synthesized as given in figure 2a and characterized using FT-IR spectroscopy, figure 2b. The characteristic imide C-N stretching at 1300 cm^{-1}, C=O stretching corresponding to carboxylic acid and ketone functionalities around 1760 cm^{-1} and 1715 cm^{-1}, and aromatic C=C (m, m) vibration at 1290 cm^{-1} were identified for PI and the FT-IR spectra of PI nanocomposite have confirmed the incorporation of the nanomaterials did not make any change in the imidization process and macromolecular structure.

3.2. Preparation of Bioreceptor

The bioreceptor preparation and biosensing strategy used in the present study is given in Figure 3a. The base response of the SAW device in the air and liquid (PBS) medium before and after the bioreceptor preparation along with one example of immunoassay analysis is given in Figure 3b. The change frequency shift was observed towards the negative range after the preparation of the bioreceptor. The average value was noted at around -14350 Hz. The decrease in SAW response is due to the transformation of SH-SAW to Love wave due to the presence of a dielectric material (polymer nanocomposite thin film) with less shear acoustic velocity than the piezoelectric SAW substrate. Changes in mass, viscoelastic, and electrical loading on the SAW device are the reasons behind the depression in frequency shift. However, for a particular device, the change in frequency shift after the bioreceptor preparation solely depends upon the mass deposition on the device since both the thickness of the polymer nanocomposite thin film and PBS flow are maintained as a constant value. The thickness of the polymer nanocomposite thin film was maintained as 600 ± 50 nm Table S1. Another notable inference is a very low increase in insertion loss.

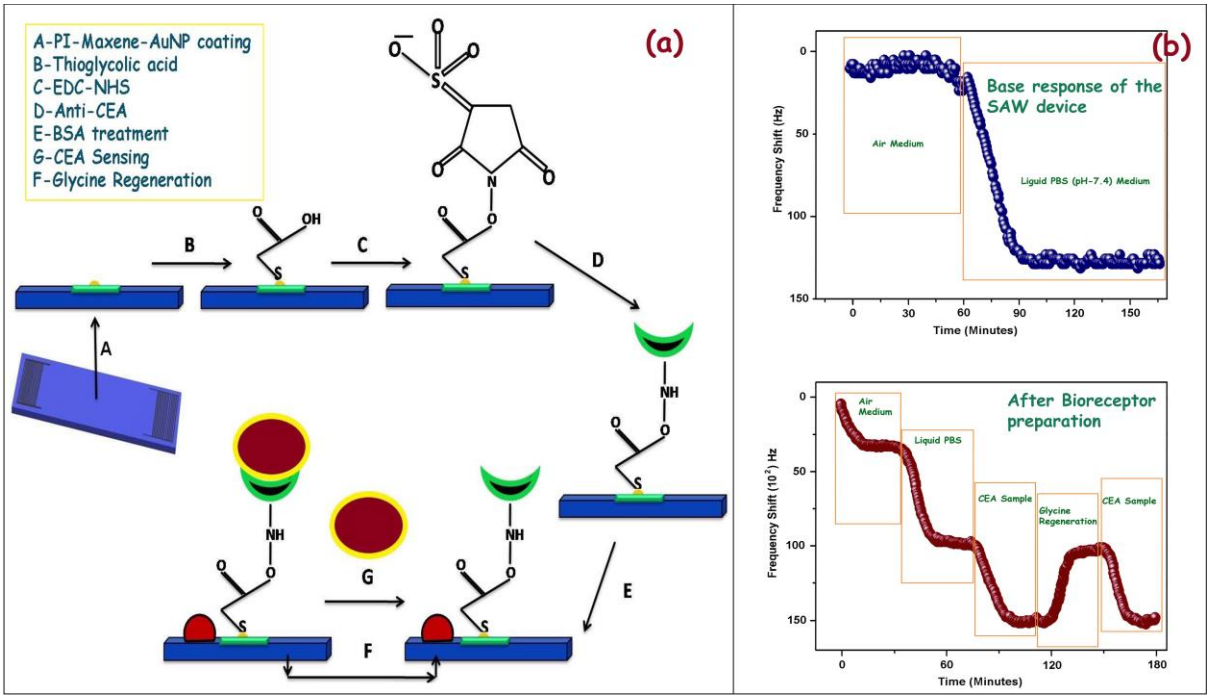

Figure 3: (a) Scheme of bioreceptor preparation and biosensing **(b)** Base performances of biosensor along with one example of immunoassay analysis

In general, any deposition on the delay line area may result abnormally increased insertion loss, which eventually makes the device unsuitable for analysis. The reason behind such increase is either due to the absorption of SAW by the new dielectric layer or by surface skimming bulk wave, acoustic wave diffracts into the bulk of the crystal resulting in high loss of energy or by a combination of both [18]. However, the thin layer used in the present study comprised of a conducting polymer polyimide and MXene-AuNP had a synergic influence on the energetically excited ∏ electron cloud within the polymer and it ultimately resulted in excellent transduction capability of the SAW device. The Peierls distortion usually restricts the ground state Π-electrons of conducting polymers as partially localized. However, in the presence of nanomaterials like MXenes, electronic excitation across the (Π – Π*) band occurs and results in a self-localized excitation within the conjugated polymers. This self-localized excitation is termed polarons, bipolarons, and solitons, which can provide uncomplicated transduction of electromagnetic waves during the immunoassay analysis [19]. In the present

study, the insertion loss was maintained at a controlled level of -24 dB after the bioreceptor preparation where the base value was reported around -20 dB.

3.3. Immunoassay response

Figures 4a and 4b represent one example of an immunoassay response against each concentration of CEA ranging from 0.1 – 100 ng/ml. Figure 4c represents the average value of immunoassay response and figure 4d, log-log calibration plot of the biosensor. The biosensor was responded linearly with the increase in the concentration of CEA solution. The limit of detection (LOD) was calculated as per our previous study and recorded at 0.001 ng/ml [20, 21]. The presence of highly transducing 2D layers of MXene in combination with AuNP provides easy passage of SAW with minimum insertion loss may be the reason for this high value of LOD in the present investigation. Regression coefficient which determines the efficiency of the biosensor was calculated at 0.9845, which is another observation to show the excellent support of the new transducing layer for high sensitivity to the biosensor. The sensitivity value was calculated at 83 Hz, which is much higher than the other reported literature [24]. The high aspect ratio AuNP can provide enough effective surface area for thioglycolic acid to react and ultimately results in a dense anti-CEA receptor concentration on the SAW device surface. Additionally, PI/MXene-AuNP thin film can provide effective transduction of SAW concerning the changes happening on the device surface. The synergic effect of the positive aspects of the conducting polymer and nanoparticle cluster ultimately resulted in excellent sensitivity and LOD for the biosensor.

The efficiency of the biosensor was tested by comparing the experimentally obtained weight of mass deposition on the device with the theoretically possible maximum values. Theoretical values are calculated by estimating the overall flow of the known concentrations of CEA solutions for a preset period. The deposited mass on the SAW device during immunoassay analysis was calculated as per the method suggested by Li et al. [20]. The results are given in

Table S2. The experimental results were in good agreement with the theoretical values and the comparison suggests the biosensor has a high analyzing potential for CEA biosensing. The analysis for reproducibility in the results was conducted as per the studies suggested by Emran et al [22]. The results are given in Figure S1 and the biosensor found excellent in consistency till the 11 runs of immunoassay measurement.

The favorability of the CEA interaction with the anti-CEA at the bioreceptor interface was evaluated theoretically using Langmuir and Freundlich isotherms as well, [23, 25, 26]. The Langmuir isotherm was plotted as C_e/q_e v/s C_e and given in Figure 4e. The CAE adsorption capacity and the energy of adsorption were calculated at 2.53 mmol/g and 2.94 L $mmol^{-1}$ respectively. Also, the adsorption and desorption coefficients (k_a and k_d) were calculated as 3298 ± 605 L mol^{-1} s^{-1} and 5.83 × 10^{-4} ± 1.12 s^{-1} [24]. The high value of ka and a non-zero kd value suggests an adsorption favourable equilibrium within the interface of anti-CEA – CEA during the immunoassay analysis. Additionally, the free energy of adsorption ($\Delta G_{sorption}$) was calculated as well at -6.84 ±0.61 kcal mol^{-1}, which also suggests favorable adsorption conditions for CEA molecules on the bioreceptor. Freundlich adsorption isotherm was plotted as ln q_e v/s ln C_e (figure 4f), isotherms suggest the sorption equilibrium of CEA on the anti-CEA bioreceptor follows Freundlich adsorption isotherm as well. The adsorption capacity was calculated at 0.658 and the intensity of adsorption at 4.14. The dimensionless constant separation factor "R_L" also was calculated at 0.956 through Freundlich isotherm parameters which also suggests the favourability of the adsorption process during the immunoassay analysis [24].

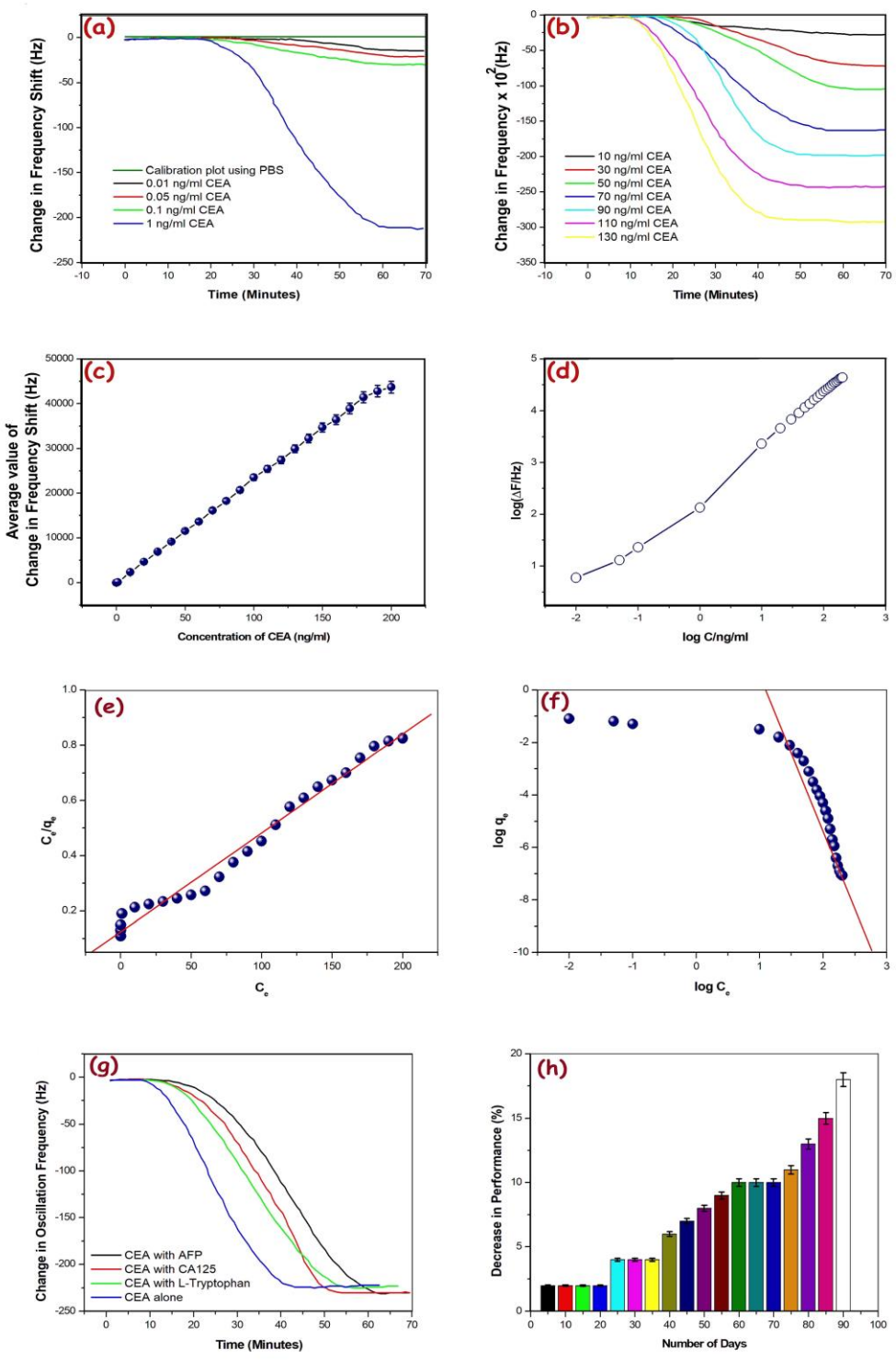

Figure 4: (a) & (b) Immunoassay response against various concentrations of CEA **(c)** Average value of change in frequency shift for each concentration **(d)** log-log calibration plot for present immunoassay analysis **(e)** Langmuir adsorption isotherm **(f)** Freundlich adsorption isotherm **(g)** Immunoassay response for selectivity study **(f)** Results of stability analysis

3.4. Analysis of clinical serum samples

The real-time analysis capability of the PI/MXene-AuNP based biosensor was conducted through clinical serum sample analysis. The study was done in collaboration with Second People's hospital, Shenzhen China. Samples were collected from the patients as a part of the primary diagnosis practice of colorectal cancer. Samples of 15 patients who underwent examination and analysis were conducted using the new biosensor in tandem with the ELISA method as well. Sample preparation was done as per the standard practice for the ELISA method, 0.5 mL serum in 2 mL of PBS solution with a pH value of 7.4. The obtained results in comparison with ELISA results are depicted in Table 1. The recorded results from the new biosensor are in excellent agreement with ELISA results with added advantages including better consistency, low analysis time, and relatively less complicated sample preparation. The standard deviations obtained are comparatively less for the biosensor than the ELISA method. ELISA method takes an average of 6-8 hours for one analysis whereas the biosensor completes the analysis within 40-60 minutes. Both the results suggest an abnormal amount of CEA concentration for 3 samples. Sample numbers 4, 7, and 13 have CEA concentrations of 33.42, 32.65, and 38.64 ng/ml respectively. These 3 patients were recommended for detailed analysis.

Table 1: Validation of the biosensor using clinical serum sample analysis

Sample No.	SAW Biosensor results (ng/ml)	ELISA (ng/ml)
1	2.56±0.25	2.63 ±0.28
2	5.25±1.00	5.30 ±1.51
3	4.56±0.55	4.51 ±0.85
4	33.42±2.50	33.43 ±4.61

5	2.51±0.54	2.55 ±0.70
6	3.50±0.25	3.53 ±0.50
7	32.65±2.51	32.58 ±4.35
8	5.68±0.37	5.65 ±0.55
9	4.25±0.36	4.65 ±0.55
10	3.46±0.25	3.40 ±0.45
11	2.45±0.35	2.50 ±0.51
12	4.32±0.35	4.30 ±0.43
13	38.64 ±3.45	37.92±4.82
14	5.65±0.49	5.58±0.55
15	6.29±1.05	6.25±1.25

3.5. The selectivity and long term stability of the biosensor

The effect of tumor marking proteins molecules including alpha-1-fetoprotein (AFP), cancer antigen 125 (CA125), and L-tryptophan on the biosensing performance was evaluated using various combinations of these samples as given in Table S3. A representative image of the analysis conducted is given in Figure 4g. The results suggest the biosensor does not have any considerable affinity towards proteins other than CEA. The equilibrium frequency shift obtained for each immunoassay run was within the range of values obtained for pure CEA solution. The long-term stability of the biosensor was analyzed for 120 days. A batch of 5 new biosensors was undergone immunoassay analysis over this period at every 5 days of intervals. The samples were stored in sterile conditions at 4°C after each immunoassay analysis. The average value of biosensing performance in terms of frequency shift was estimated in comparison with the initial day value. The percentage of decrease in a frequency

shift of the immunoassay response is depicted in Figure 4h. The results were within the range of standard deviation obtained for initial day analysis for about 35th days. Further, the values started deviating slowly and from the 75th day, the value has varied abruptly.

4. Conclusion

A novel polymer nanocomposite thin film was synthesized and successfully utilized as a transuding bioreceptor a thin film for a liquid state love mode SAW biosensor for the selective detection of CEA. The nanocomposite film was comprised of a novel formulation of PI/MXene-AuNP. MXene 2D layer was successfully prepared and TEM imaged in the present study. The PI nanocomposite thin film was coated on the delay line area of the SAW device specifically prepared for this study through the photolithography method using an AT quartz crystal. Conducting a polymer-based nanocomposite system has been well supported to overcome the usual hurdle of high insertion loss for polymer-based SAW analysis. The inherent quality of the conducting polymers, MXene, and AuNP has allowed the passage of love wave from the input to output IDT through the polymer nanocomposite coated delay line of the SAW device without much loss in intensity. A maximum increase in insertion loss at 8 dB was recorded for PI nanocomposite coating. Further, the bioreceptor of a self-assembled monolayer of anti-CEA was prepared via thioglycolic acid – EDC/NHS mechanism. The high aspect ratio AuNP's were acted like active reaction sites for thioglycolic acid attack and facilitate the formation of a dense biofilm of an anti-CEA monolayer on the PI nanocomposite thin film. This ultimately results in a positive effect on the sensitivity and stability of the biosensor. The biosensor was validated for CEA sensing using a specially designed sample micro-fluidic system and a network analyzer. The biosensor has recorded a limit of detection value at 0.001 ng/ml and upper saturation point of 120 ng/ml of CEA concentration. With the support of good transduction capability of MXene coupled with PI conducting polymer, the sensitivity in terms of variation in oscillation frequency w.r.t the

base frequency of the bioreceptor was reported excellent for each sample of CEA. The biosensor has reported excellent selectivity towards CEA and showed the least affinity towards the common tumor marking proteins like AFP, CA 125, and L-tryptophan. Another notable outcome of the present study is the exceptional stability of the present biosensor. The biosensor exhibited stable performance around 75 days without reporting much decrease in biosensing performance. The adsorption parameters like K_a and K_d were calculated as 3298 ± 605 L mol^{-1} s^{-1} and 5.83 10^{-4} ± 1.28 × s^{-1} respectively using Langmuir adsorption isotherm. The nonzero K_d value has suggested the existing equilibrium between the forward and backward reactions. The free energy of adsorption was estimated as -6.54 ±0.61 kcal mol^{-1}, which also suggests a favorable condition for antigen-antibody interaction. The findings were further confirmed using Freundlich adsorption isotherm as well.

Acknowledgement

We express our sincere gratitude to our funding agencies Research and Development Program of Guangdong Province (Grant no. 2020B0101040002), Key Research Program of Education Department for Guangdong Province, (Grant no. 2020ZDZX2007), Shenzhen Science & Technology Project (Grant nos. JCYJ20180507182106754, JCYJ2018050718243957，JCYJ20180305124317872, GJHZ20200073109583010).

Prof. Honey John, Department of Polymer Science and Rubber Technology, Cochin University of Science and Technology, for giving access to her laboratory and her support as a mentor.

Conflict of interest

There is no conflict of interest in connection with this research work.

Data Availability Statement

The raw/processed data required to reproduce these findings cannot be shared at this time as the data also forms part of an ongoing study.

References

1. V.W. Brar, A.R. Koltonow, J. Huang, New Discoveries and Opportunities from Two-Dimensional Materials, ACS Photonics, 4 (2017) 407-411.
2. C. Ashworth, 2D Materials: The thick and the thin, Nature Reviews Materials, 3 (2018) Article number: 18019.
3. A. Szuplewska, D. Kulpińska, A. Dybko, M. Chudy, A.M. Jastrzębska, A. Olszyna, Z. Brzózka, Future Applications of MXenes in Biotechnology, Nanomedicine, and Sensors, Trends in Biotechnology, https://doi.org/10.1016/j.tibtech.2019.09.001.
4. H. Liu, C. Duan, C. Yang, W. Shen, F. Wang, Z. Zhu, A novel nitrite biosensor based on the direct electrochemistry of hemoglobin immobilized on MXene-Ti3C2, Sensors and Actuators B: Chemical, 218 (2015) 60-66.
5. Y.V. Stebunov, O.A. Aftenieva, A.V. Arsenin, V.S. Volkov, Highly Sensitive and Selective Sensor Chips with Graphene-Oxide Linking Layer, ACS Appl. Mater. Interfaces, 7 (2015) 21727-21734.

6. Y. Ma, Y. Yue, H. Zhang, F. Cheng, W. Zhao, J. Rao, S. Luo, J. Wang, X. Jiang, Z. Liu, N. Liu, Y. Gao, 3D Synergistical MXene/Reduced Graphene Oxide Aerogel for a Piezoresistive Sensor, ACS Nano, 12 (2018) 3209-3216.
7. S. Su, Q. Sun, X. Gu, Y. Xu, J. Shen, D. Zhu, J. Chao, C. Fan, L. Wang, Two-dimensional nanomaterials for biosensing applications, TrAC Trends in Analytical Chemistry, 119 (2019) 115610.
8. W. Wen, Y. Song, X. Yan, C. Zhu, D. Du, S. Wang, A.M. Asiri, Y. Lin, Recent advances in emerging 2D nanomaterials for biosensing and bioimaging applications, Materials Today, 21 (2018) 164-177.
9. Q. Wu, N. Li, Y. Wang, Y. liu, Y. Xu, S. Wei, J. Wu, G. Jia, X. Fang, F. Chen, X. Cui, A 2D transition metal carbide MXene-based SPR biosensor for ultrasensitive carcinoembryonic antigen detection, Biosensors and Bioelectronics, 144 (2019) 111697.
10. Y. Guo, M. Zhong, Z. Fang, P. Wan, G. Yu, A Wearable Transient Pressure Sensor Made with MXene Nanosheets for Sensitive Broad-Range Human–Machine Interfacing, Nano Lett. 19 (2019) 1143-1150.
11. R. Li, L. Zhang, L. Shi, P. Wang, MXene Ti3C2: An Effective 2D Light-to-Heat Conversion Material, ACS Nano, 11 (2017) 3752-3759.
12. X. Huang, R. Wang, T. Jiao, G. Zou, F. Zhan, J. Yin, L. Zhang, J. Zhou, Q. Peng, Facile Preparation of Hierarchical AgNP-Loaded MXene/Fe3O4/ Polymer Nanocomposites by Electrospinning with Enhanced Catalytic Performance for Wastewater Treatment, ACS Omega, 4 (2019) 1897-1906.
13. G.T. Chandran, X. Li, A. Ogata, R.M. Penner, Electrically Transduced Sensors Based on Nanomaterials, Anal. Chem. 89 (2017) 249-275.

14. Y. Ding, T. Xu, O. Onyilagha, H. Fong, Z. Zhu, Recent Advances in Flexible and Wearable Pressure Sensors Based on Piezoresistive 3D Monolithic Conductive Sponges, ACS Appl. Mater. Interfaces, 11 (2019) 6685-6704.
15. N. Fourati, M. Seydou, C. Zerrouki, A. Singh, S. Samanta, F. Maurel, D.K. Aswal, M. Chehimi, Ultrasensitive and Selective Detection of Dopamine Using Cobalt-Phthalocyanine Nanopillar-Based Surface Acoustic Wave Sensor, ACS Appl. Mater. Interfaces, 6 (2014) 22378-22386.
16. M.A. Iqbal, A. Tariq, A. Zaheer, S. Gul, S.I. Ali, M. Z. Iqbal, D. Akinwande, S. Rizwan, Ti3C2-MXene/Bismuth Ferrite Nanohybrids for Efficient Degradation of Organic Dyes and Colorless Pollutants, ACS Omega, 4 (2019) 20530–20539.
17. S.A. Aromal, D. Philip, Green synthesis of gold nanoparticles using Trigonella foenum-graecum and its size-dependent catalytic activity, Spectrochimica Acta Part A: Molecular and Biomolecular Spectroscopy, 97 (2012) 1–5.
18. D.S. Ballantine, Jr.H. Wohltjen, Elastic Properties of Thin Polymer Films Investigated with Surface Acoustic Wave Devices, Chemical Sensors and Microinstrumentation, ACS Symposium Series, 403 (1989) 222-236.
19. Y.F. Lin, C.H. Chen, W.J. Xie, S.H. Yang, C.S. Hsu, M.T. Lin, W.B. Jian, Nano Approach Investigation of the Conduction Mechanism in Polyaniline Nanofibers, ACS Nano, 5 (2011) 1541-1548.
20. S. Li, Y. Wan, Y. Su, C. Fan, V.R. Bhethanabotla, Gold nanoparticle-based low limit of detection Love wave biosensor for carcinoembryonic antigens, Biosensors and Bioelectronics, 95 (2017) 48–54.
21. P.J. Jandas, J. Luo, A. Quan, C. Li, C. Fu, Y.Q. Fu, Graphene oxide-Au nano particle coated quartz crystal microbalance biosensor for the real time analysis of carcinoembryonic antigen, RSC Advances, 10 (2020) 4118.

22. M.Y. Emran, S.A. El-Safty, M.A. Shenashen, T. Minowa, A well-thought-out sensory protocol for screening of oxygen reactive species released from cancer cells, Sens Actuators B Chem, 284 (2019) 456–467.
23. F. Temel, E. Ozcelik, A.G. Ture, M. Tabakci, Sensing abilities of functionalized calix[4]arene coated QCM sensors towards volatile organic compounds in aqueous media, Applied Surface Science, 412 (2017) 238–251.
24. M. Yang, M. Thompson, W.C. Duncan-Hewitt, Interfacial Properties and the Response of the Thickness-Shear-Mode Acoustic Wave Sensor in Liquids, Langmuir, 9 (1993) 802-811.
25. P.J. Jandas, J. Luo, A. Quan, C. Qiu, W. Cao, C. Fu, Y.Q. Fu, Highly selective and label-free Love-mode surface acoustic wave biosensor for carcinoembryonic antigen detection using a self-assembled monolayer bioreceptor, Applied Surface Science, 518 (2020) 146061.
26. P.J. Jandas, J. Luo, K. Prabakaran, F. Chen, Y.Q. Fu, Highly stable, love-mode surface acoustic wave biosensor using Au nanoparticle-MoS_2-rGO nano-cluster doped polyimide nanocomposite for the selective detection of carcinoembryonic antigen, Material Chemistry and Physics, 246 (2020) 122800.